Clinical, Cosmetic and Investigational Dermatology

Dovepress
Taylor & Francis Group

Open Access Full Text Article

ORIGINAL RESEARCH

Network Pharmacology and Animal Experimental Validation on the Therapeutic Mechanisms of *Prunus cerasifera* Extract in Psoriasis

Huiqin Wang[1], Yuan Ding[1], Zhenrui Wang[1], Yiqi Wang[1], Yanwen Liu[2], Yaqin Ma[1], Weidong Wu[1]

[1]Department of Dermatology and Venereology, People's Hospital of Xinjiang Uygur Autonomous Region, Xinjiang Clinical Research Center for Dermatology and Venereology, Xinjiang Key Laboratory of Dermatology Research, Urumqi, Xinjiang Uygur Autonomous Region, 830000, People's Republic of China; [2]Xinjiang Medical University, Urumqi, Xinjiang Uygur Autonomous Region, 830000, People's Republic of China

Correspondence: Weidong Wu, Department of Dermatology and Venereology, People's Hospital of Xinjiang Uygur Autonomous Region, Xinjiang Clinical Research Center for Dermatology and Venereology, Xinjiang Key Laboratory of Dermatology Research, No. 91, Tianchi Road, Tianshan District, Urumqi, Xinjiang Uygur Autonomous Region, 830000, People's Republic of China, Email xiaobenshu2003@sina.com

Background: Psoriasis is a chronic immune-mediated inflammatory skin disorder characterized by excessive keratinocyte proliferation and persistent inflammation. Its multifactorial pathogenesis involves complex inflammatory mediators and signaling pathways. Current treatments remain limited by high recurrence and adverse effects, highlighting the need for safe and effective natural bioactive compounds for psoriasis prevention and management. In addition, cyclin B1 (CCNB1) has been reported as a hub gene associated with psoriasis; however, its mechanism of action remains unclear.

Objective: To elucidate the potential therapeutic mechanisms of a bioactive extract derived from *Prunus cerasifera* fruit powder (PCE10) by integrating network pharmacology and animal experimental validation.

Methods: A psoriasis-like mouse model was established using imiquimod (IMQ) in mice as the study subjects. The anti-psoriatic effect of PCE10 was assessed using the Psoriasis Area and Severity Index (PASI), histopathological examination, and inflammatory cytokine assays. Network pharmacology combined with machine learning algorithms was employed to identify psoriasis-associated target genes potentially regulated by PCE10. Molecular docking were subsequently performed to predict the binding interactions between candidate bioactive compounds and key molecular targets.

Results: Network pharmacology identified 67 psoriasis-related targets, with 23 hub genes detected in the protein-protein interaction network. Enrichment analyses indicated involvement in inflammatory regulation and TNF, NF-κB, and p53 pathways. Machine learning identified CCNB1 as a key psoriasis-associated gene. Molecular docking indicated interactions between p53 and the bioactive compounds of PCE10. In vivo, PCE10 alleviated IMQ-induced psoriasis-like dermatitis and reduced epidermal hyperplasia, decreasing serum levels of IL-23, IL-17A, and TNF-α. Mechanistically, PCE10 suppressed keratinocyte proliferation by modulating the p53/CCNB1 axis.

Conclusion: PCE10 may exert anti-psoriatic effects through modulation of p53/CCNB1 regulatory axis. Nevertheless, this study is mainly based on an IMQ-induced mouse model and is not supported by validation in human psoriatic skin tissues or clinical specimens. Additional translational studies are required to establish its clinical applicability.

Keywords: psoriasis, imiquimod, *Prunus cerasifera*, network pharmacology, machine learning

Introduction

Psoriasis is a chronic, immune-mediated inflammatory skin disorder characterized by hyperproliferation of keratinocytes, aberrant differentiation, and persistent cutaneous inflammation.[1] Affecting approximately 2–3% of the global population, psoriasis not only imposes substantial physical discomfort but also significantly impacts patients' psychological well-being and quality of life.[2] Psoriasis arises from a multifaceted pathogenic process characterized by abnormal crosstalk between immune cells and keratinocytes, with multiple inflammatory mediators and signaling pathways contributing to disease onset and progression.[3] The pathogenesis of psoriasis is driven by a complex network of signaling pathways,

https://doi.org/10.2147/CCID.S608837
Received: 12 March 2026
Accepted: 13 June 2026
Published: 27 June 2026

including the nuclear factor kappa-B (NF-κB), Janus kinase/signal transducer and activator of transcription (JAK-STAT), and p53 pathways, which collectively regulate inflammation, keratinocyte hyperproliferation, and apoptosis.[4] Key inflammatory cytokines, including interleukin (IL)-17A, IL-23, and tumor necrosis factor-α (TNF-α), drive keratinocyte proliferation and sustain the chronic inflammatory milieu, making them critical therapeutic targets.[5] The central role of the IL-23/IL-17 axis in psoriasis pathogenesis has been well established, and IL-17 inhibitors have emerged as effective biologic therapies for moderate-to-severe psoriasis.[6] Despite the availability of topical, systemic, and biologic therapies, current treatment strategies are limited by high recurrence rates, long-term adverse effects, and financial burden.[7] These challenges underscore the necessity for safer and more accessible therapeutic options, especially natural products capable of targeting multiple biological pathways. Increasing evidence suggests that plant-derived bioactive compounds can effectively regulate inflammatory signaling and cell proliferation in a range of skin disorders,[8] offering potential as complementary or alternative therapies for psoriasis.

Prunus cerasifera, commonly known as cherry plum, is a fruit-bearing plant widely recognized for its nutritional and medicinal properties, including anti-inflammatory and antioxidant effects.[9] Emerging evidence suggests that *Prunus cerasifera*-derived components can modulate cellular signaling and immune responses,[10] yet their therapeutic potential in psoriasis remains largely unexplored. Leveraging computational methods enables the identification of feature genes like Cyclin B1 (CCNB1) from complex datasets, providing mechanistic insights into disease modulation. CCNB1 was selected for investigation based on its established role in cell cycle regulation and preliminary bioinformatic screening that identified it as a hub gene potentially associated with psoriasis pathogenesis.[11] CCNB1, a key regulator of cell cycle progression, has been implicated in abnormal keratinocyte proliferation and psoriasis.[12] Dysregulation of the p53/CCNB1 axis contributes to uncontrolled cellular proliferation and inflammation in skin disorders,[13] making CCNB1 a potential therapeutic target for psoriasis.

This study hypothesized that the ethanol extract of *Prunus cerasifera* fruit powder (PCE10) could alleviate psoriasis-like skin inflammation possibly by targeting p53/CCNB1 axis. Through the combined application of network pharmacology, machine learning, molecular docking, and experimental verification, this study seeks to comprehensively assess the anti-psoriatic potential of PCE10, clarify its molecular mechanisms, and establish a theoretical foundation for developing new natural-product-based therapies.

Materials and Methods

Preparation of PCE10

Prunus cerasifera was purchased from Qingzhi Biotechnology company (Xi'an, China) and identified by Professor Xiaoying Liu from Xinjiang University. A voucher specimen (No. 20250001F) was deposited at the College of Life Sciences and Technology, Xinjiang University. The ethanol extract of *Prunus cerasifera* fruit powder (designated as PCE10) was prepared using ethanol extraction combined with macroporous resin purification. Briefly, the dried and pulverized *Prunus cerasifera* fruit powder was extracted at a solid-to-liquid ratio of 1:20 (g/mL) with 70% ethanol. The mixture underwent ultrasonic extraction (600 W, 20 min), followed by water-bath extraction at 60°C for 2 h. After filtration, the residue was extracted once more under identical conditions. The combined filtrate was concentrated using a vacuum rotary evaporator to obtain the crude ethanol extract. The crude extract was then preliminarily separated and purified using macroporous adsorption resin. D101 resin was used as the carrier, and the wet resin was loaded into a column by the wet packing method with ethanol. After sample loading and adsorption for 12 h, elution was performed using a low-concentration ethanol solvent. The eluate was concentrated using a rotary evaporator and subsequently freeze-dried into powder using a vacuum freeze dryer to obtain PCE10. The chemical composition of PCE10 was characterized using ultra-high performance liquid chromatography-quadrupole-orbitrap mass spectrometry (UPLC-Q-Orbitrap MS/MS).

Experimental Animals

Seven-week-old C57BL/6 mice were obtained from the Experimental Animal Center of Xinjiang Medical University (Urumqi, Xinjiang, China). All animal procedures were approved by the Ethics Committee of People's Hospital of

Xinjiang Uygur Autonomous Region (approval no. KY2024102201). The animal experiments were conducted in accordance with the Guide for the Care and Use of Laboratory Animals and the ARRIVE guidelines. After one week of acclimation, mice were randomly assigned to six groups (n=6 per group): Control, imiquimod (IMQ), low-dose PCE10 (PCE10-L; 75 mg/kg/day), medium-dose PCE10 (PCE10-M; 150 mg/kg/day), high-dose PCE10 (PCE10-H; 300 mg/kg/day), and positive control methotrexate (MTX, 1 mg/kg/day). The dorsal hair was shaved. All groups except the Control group were topically applied 62.5 mg of IMQ daily for six consecutive days. Control mice received an equal amount of Vaseline. Treatments were administered by oral gavage daily with the corresponding doses of PCE10 or MTX. Body weight and psoriasis severity were monitored daily using the Psoriasis Area and Severity Index (PASI), which evaluates erythema, scaling, and skin thickness. Each parameter was scored on a 0–4 scale. At study endpoint, mice were euthanized by intraperitoneal injection of 150 mg/kg pentobarbital sodium (Sigma-Aldrich, St. Louis, MO, USA), and skin and spleen tissues were collected.

Histological and Immunohistochemical (IHC) Analyses

Skin specimens were fixed with paraformaldehyde and subsequently dehydrated in a graded ethanol series before paraffin embedding. After sectioning, the slides were stained with hematoxylin and eosin (HE; G1120, Solarbio, Beijing, China) for histopathological examination, dehydrated through ethanol, cleared with xylene, and mounted with neutral resin. Histological changes were monitored and recorded microscopically. Epidermal thickness was measured using ImageJ software.

For IHC staining, paraffin sections were first deparaffinized using xylene and then rehydrated through descending concentrations of ethanol. Antigen retrieval was conducted in sodium citrate buffer, followed by quenching of endogenous peroxidase activity using 3% hydrogen peroxide. Non-specific binding was blocked by incubation with 5% BSA for 30 min. Sections were incubated overnight at 4°C with Ki67 primary antibody (1:1000, 28,074-1-AP, Proteintech, Wuhan, China), washed with phosphate-buffered saline, and incubated with horseradish peroxidase (HRP)-conjugated secondary antibody (1:2000, 65–6120, Thermo Fisher Scientific, Waltham, MA, USA). Signal visualization was achieved with DAB substrate (DA1016, Solarbio). The sections were then counterstained with hematoxylin, dehydrated, cleared, and mounted before microscopic imaging. Quantification of positively stained cells was performed using ImageJ software.

ELISA

Serum was separated by centrifugation, and levels of IL-17A (E-MSEL-M0006, Elabscience, Wuhan, China), TNF-α (PT512, Beyotime, Shanghai, China), and IL-23 (EK0512, Signalway Antibody, Maryland, USA) were determined using ELISA kits according to manufacturer instructions.

Western Blotting (WB)

Tissue samples were homogenized in (RIPA buffer supplemented with protease and phosphatase inhibitors. Protein concentrations were determined using a BCA protein assay kit (P0012, Beyotime). Equal amounts of protein were denatured, separated by SDS-PAGE, and transferred to PVDF membranes, which were subsequently blocked with 5% BSA prior to incubation overnight at 4°C with primary antibodies against p53 (1:1000, MA5-37923, Thermo Fisher Scientific), CCNB1 (1:1000, 55,004-1-AP, Proteintech), and glyceraldehyde 3-phosphate dehydrogenase (GAPDH; 1:5000, MA5-35235, Thermo Fisher Scientific). Membranes were washed, incubated with HRP-conjugated secondary antibody (1:2000, 65–6120, Thermo Fisher Scientific) at room temperature for 1 h, and visualized using enhanced chemiluminescence (P0018S, Beyotime). Relative protein expression was quantified using ImageJ software with GAPDH as the internal reference.

UPLC-Q-Orbitrap MS/MS

Qualitative characterization of the chemical constituents in PCE10 was performed using a qDionex UltiMate 3000 UPLC-Q-Orbitrap MS/MS system (Thermo Fisher Scientific). Chromatographic separation of the analytes was performed on a Waters ACQUITY UPLC HSS T3 column (Waters Corporation, Milford, MA, USA), with the column

temperature maintained at 50 °C throughout the analysis. Mass spectrometric analysis was conducted using a quadrupole–Orbitrap mass spectrometer equipped with a heated electrospray ionization (HESI) source. Samples were analyzed in both positive and negative ionization modes. The data-dependent acquisition parameters for full-scan MS were set as follows: spray voltage 3.5 kV in positive mode and 2.5 kV in negative mode; sheath gas 50 arbitrary units (arb); auxiliary gas 10 arb; sweep gas 1 arb; ion transfer tube temperature 325°C; and vaporizer temperature 350°C. The full-scan mass spectra were acquired at a resolution of 60,000, with a scanning range of m/z 67–1000. MS/MS spectra were obtained using data-dependent acquisition with a resolution of 30,000 and an isolation window of 1 m/z.

Bioactive Compound Screening and Target Prediction

The chemical constituents identified by UPLC–Q-Orbitrap MS/MS were searched in the PubChem database to obtain their corresponding SMILES structures. These structures were then submitted to the SwissADME platform to predict their pharmacokinetic characteristics and drug-likeness to screen potential bioactive compounds. Compounds were considered potential candidates when they exhibited high predicted gastrointestinal absorption and satisfied at least two of the following drug-likeness rules: Lipinski, Ghose, Veber, Egan, and Muegge. The selected bioactive compounds were subjected to target prediction using the SwissTargetPrediction database (http://www.swisstargetprediction.ch/), and predicted targets with probability > 0 were collected for subsequent analyses.

Identification of Psoriasis-Related Targets

Psoriasis-associated gene expression data were obtained from the Gene Expression Omnibus (GEO) database (https://www.ncbi.nlm.nih.gov/gds/) using the dataset GSE13355, which includes 64 normal skin samples and 58 psoriasis skin samples. DEGs were determined using the thresholds $|\log_2 \text{fold change}| > 1$ and adjusted P value < 0.01. Screened DEGs were considered psoriasis-related targets. In addition, psoriasis-associated targets were retrieved from the GeneCards database (http://www.genecards.org/) using the keyword "psoriasis."

Construction of the Drug–Component–Disease Target Network

The intersection between PCE10-related targets and psoriasis-associated targets was determined using a Venn diagram. A visualized drug–component–disease target network was constructed using Cytoscape version 3.10.1. In this network, nodes represent drugs, components, or targets, whereas edges represent the interactions among them.

Gene Ontology (GO) and Kyoto Encyclopedia of Genes and Genomes (KEGG) Pathway Enrichment Analyses

The predicted therapeutic targets of PCE10 for psoriasis were subjected to GO and KEGG enrichment analyses using the Bioinformatics online platform. The top ten significantly enriched terms in each category were selected for presentation.

Protein-Protein Interaction (PPI) Network and Identification of Hub Targets

Potential therapeutic targets of PCE10 were uploaded to the STRING database (https://www.string-db.org/) with the species limited to *Homo sapiens*. To construct the PPI network, the minimum required interaction score was set to ≥ 0.4. The resulting network was visualized using Cytoscape software, and topological analysis was conducted using the cytoNCA plugin. Hub targets within the network were determined according to the median values of multiple topological parameters (Betweenness, Closeness, Degree, and Eigenvector Centralities; Local Average Connectivity, Network Centrality).

Identification of Feature Genes Based on Machine Learning Algorithms

Using the gene expression matrix of the GSE13355 dataset, machine learning algorithms were implemented in R software using the packages glmnet, e1071, kernlab, caret, randomForest, limma, and ggpubr. LASSO regression, SVM-RFE, and random forest analyses were performed to identify feature genes among the key targets. The intersection

of the results obtained from the three algorithms was defined as the feature genes associated with PCE10 treatment in psoriasis.

Molecular Docking

Structures of core bioactive compounds were obtained from the PubChem database, while the crystallographic structures of target proteins were downloaded from the RCSB Protein Data Bank (https://www.rcsb.org/). Protein structures were pretreated in PyMOL version 3.1.4.1 by removing water molecules and adding hydrogen atoms. Molecular docking analysis was subsequently performed using AutoDock Vina version 1.2.5, and the docking conformations were visualized with PyMOL version 3.1.4.1.

Statistical Analysis

All quantitative results are presented as the mean ± standard error of the mean (SEM). Statistical analyses were carried out using GraphPad Prism version 10.1.2. Comparisons among three or more groups were conducted using one-way or two-way analysis of variance (ANOVA) followed by Tukey's post hoc test. A p-value < 0.05 was considered statistically significant.

Results

PCE10 Ameliorates IMQ-Induced Psoriasis-Like Lesions and Histopathological Changes

Psoriasis-like dermatitis was induced in C57BL/6 mice using topical IMQ and treated with different doses of PCE10. Gross observation of dorsal skin revealed that IMQ-treated mice developed marked erythema, scaling, and thickening, hallmarks of psoriasis-like lesions. Administration of PCE10 or MTX significantly improved these skin lesions, manifested as reduced erythema, decreased scaling, and diminished skin thickness. The PCE10-M and PCE10-H groups exhibited more pronounced improvement than the PCE10-L group (Figure 1A). PASI scoring confirmed these observations (Figure 1B–E). HE staining further demonstrated pronounced epidermal hyperplasia in the IMQ group, which was alleviated after PCE10 intervention (Figure 1F–G).

PCE10 Mitigates IMQ-Induced Systemic Effects and Inflammation

Compared to the Control group, IMQ treatment caused significant body weight loss in mice, which was partially reversed by PCE10 or MTX administration (Figure 2A). IMQ-induced splenomegaly was evident in the model group, with a significantly increased spleen index; PCE10 and MTX treatment reduced the spleen index (Figure 2B and C). ELISA revealed elevated serum levels of IL-17A, TNF-α, and IL-23 following IMQ treatment, which were significantly decreased by PCE10 or MTX intervention (Figure 2D).

Identification of PCE10 Components and Target Prediction

Using UPLC-Q-Exactive Orbitrap MS/MS, 230 components were identified in PCE10 (Figure 3A and B). SwissADME analysis screened 133 potential bioactive constituents (Table 1), and SwissTargetPrediction predicted 898 potential PCE0 targets. Differential expression analysis of the GSE13355 dataset revealed genes that are dysregulated in psoriasis and identified as potential DEGs (Figure 4A). Integrating GeneCards data (6057 DEGs) and intersecting with PCE10 targets, 67 therapeutic targets were identified (Figure 4B). The drug–component–disease target network was constructed and visualized using Cytoscape version 3.10.1., revealing *quercetin, emodin, isorhamnetin*, and *citroflex 4* as core bioactive compounds (Figure 4C).

Enrichment Analysis results

GO results indicated that the targets were primarily involved in biological processes such as xenobiotic response, regeneration, and inflammation regulation. Cellular components included protein kinase complexes, spindle microtubules, and mitochondrial outer membrane. Molecular functions were associated with serine/threonine kinase activity,

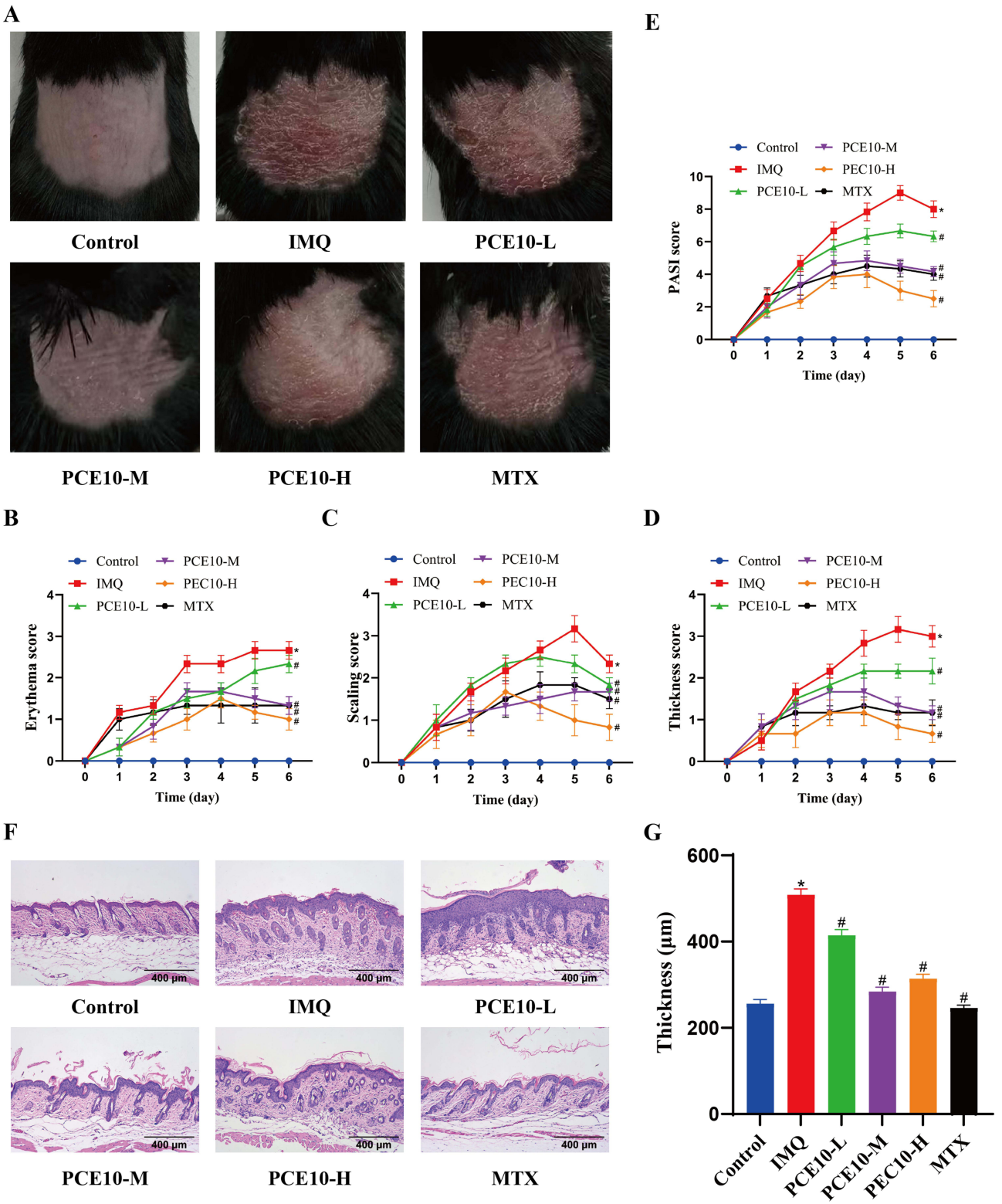

Figure 1 PCE10 alleviates IMQ-induced psoriasis-like skin phenotype. (**A**) Representative dorsal skin images of mice. (**B**) Erythema severity score. (**C**) Scaling severity score. (**D**) Infiltration severity score of affected skin area. (**E**) PASI score of dorsal skin. (**F**), HE-stained skin sections. (**G**) Quantification of epidermal thickness. Data analyzed by one-way or two-way ANOVA with Tukey's post hoc test. n = 6 mice per group; *$p < 0.05$ vs Control; #$p < 0.05$ vs IMQ.

https://doi.org/10.2147/CCID.S608837

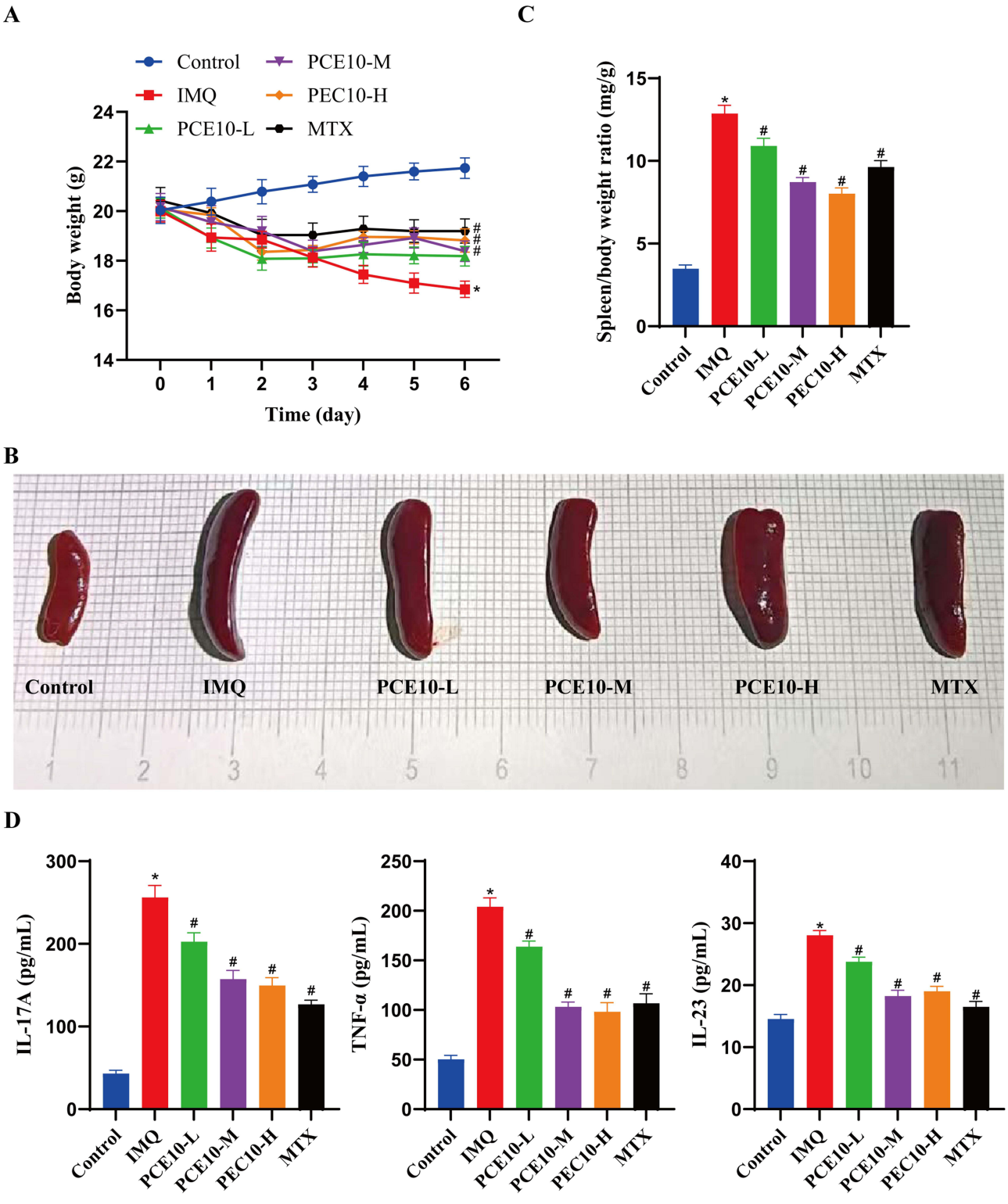

Figure 2 PCE10 attenuates IMQ-induced body weight loss, splenic changes, and inflammation. (**A**) Body weight of mice. (**B** and **C**) Representative images of mouse spleens (**B**) and spleen index (**C**). (**D**) Serum levels of IL-17A, TNF-α, and IL-23 measured by ELISA. Data analyzed by one-way or two-way ANOVA with Tukey's post hoc test. n = 6 mice per group; *$p < 0.05$ vs Control; #$p < 0.05$ vs IMQ.

https://doi.org/10.2147/CCID.S608837

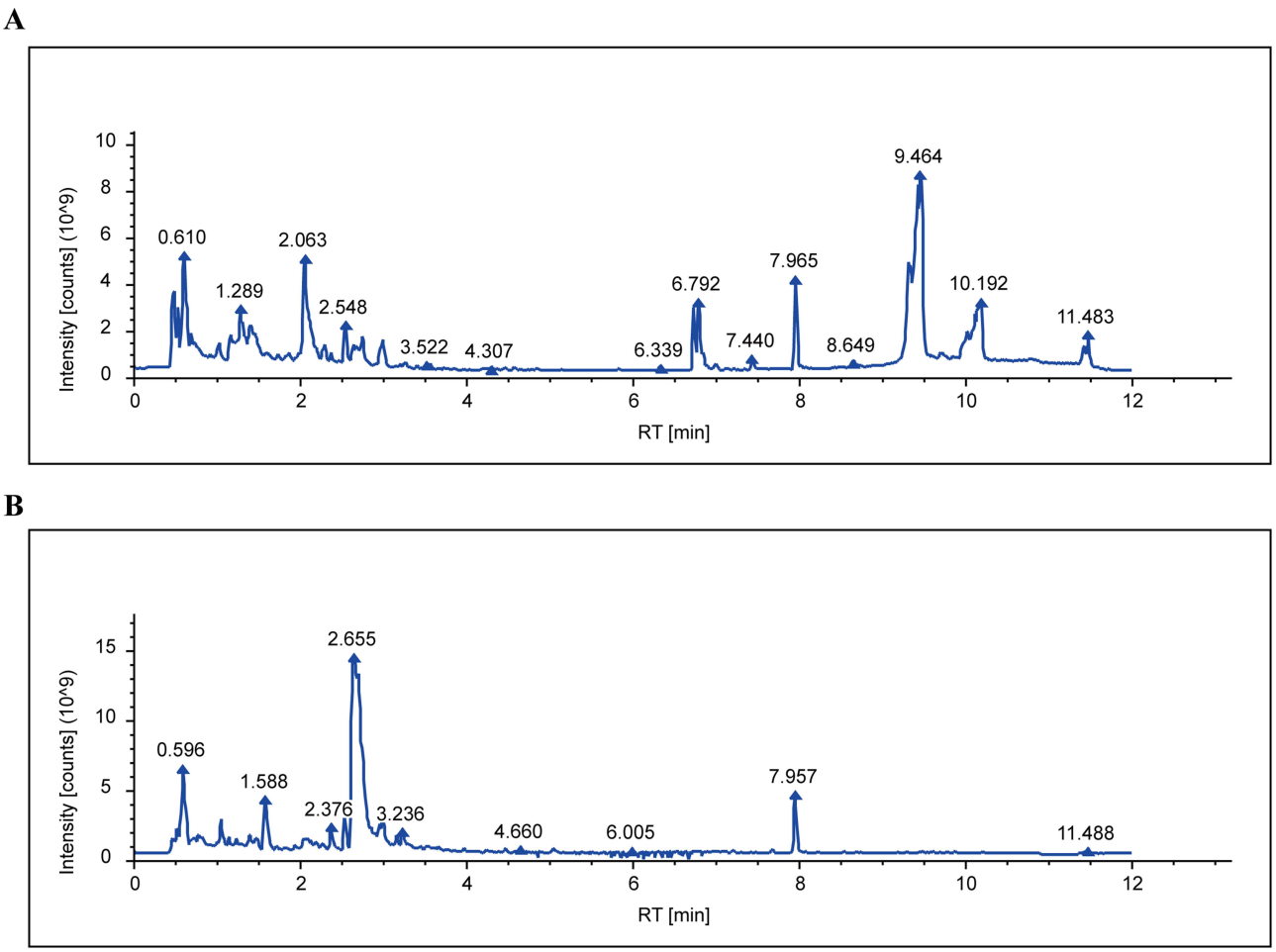

Figure 3 Prediction of PCE10 therapeutic targets. (**A**) Base peak chromatogram of PCE10 in positive ion mode. (**B**) Base peak chromatogram of PCE10 in negative ion mode.

transcription factor activity, and DNA binding, indicating potential regulation of kinase signaling and inflammation (Figure 5A). KEGG pathway analysis revealed enrichment in TNF, NF-κB, and p53 signaling pathways, apoptosis, cellular senescence, and AGE-RAGE signaling, suggesting involvement in inflammation, proliferation, apoptosis, and oxidative stress regulation (Figure 5B).

Table 1 Active Chemical Constituents of PCE10

No.	Ion Mode	Name	Formula	Measured m/z	Retention Times (min)
1	pos	L-Norleucine	C6 H13 N O2	132.10151	1.404
2	pos	alpha-Aspartylphenylalanine	C13 H16 N2 O5	281.11229	2.768
3	pos	Aspartame	C14 H18 N2 O5	295.12806	3.574
4	pos	DL-Stachydrine	C7 H13 N O2	144.1014	0.683
5	pos	Citroflex A-4	C20 H34 O8	425.21326	9.361
6	pos	Isoleucine	C6 H13 N O2	132.1015	1.32
7	pos	Quercetin	C15 H10 O7	303.04915	5.054

(*Continued*)

https://doi.org/10.2147/CCID.S608837

Table 1 (Continued).

No.	Ion Mode	Name	Formula	Measured m/z	Retention Times (min)
8	pos	Meleagrin	C23 H23 N5 O4	434.18126	5.05
9	pos	Adenine	C5 H5 N5	136.0613	0.692
10	pos	Valine	C5 H11 N O2	118.08588	0.983
11	pos	Xanthohumol	C21 H22 O5	355.15276	7.962
12	pos	Leucylproline	C11 H20 N2 O3	229.15399	2.76
13	pos	Mevalonolactone	C6 H10 O3	131.06992	1.621
14	pos	Xanthurenic acid	C10 H7 N O4	206.04427	2.591
15	pos	Proline	C5 H9 N O2	116.0702	0.655
16	pos	Kynurenic acid	C10 H7 N O3	190.04934	2.821
17	pos	Valylproline	C10 H18 N2 O3	215.13845	2.038
18	pos	4-Acetamidobutanoic acid	C6 H11 N O3	129.05427	1.496
19	pos	Guanine	C5 H5 N5 O	152.05624	1.032
20	pos	3-(1-hydroxyethyl)-2,3,6,7,8,8a-hexahydropyrrolo[1,2-a]pyrazine-1,4-dione	C9 H14 N2 O3	199.10719	1.882
21	pos	Hypoxanthine	C5 H4 N4 O	137.04538	1.161
22	pos	Caprolactam	C6 H11 N O	114.09103	2.93
23	pos	cis,cis-Muconic acid	C6 H6 O4	143.03345	1.334
24	pos	N-Acetylputrescine	C6 H14 N2 O	131.11748	0.68
25	pos	Prolylleucine	C11 H20 N2 O3	229.15404	2.532
26	pos	3-Aminosalicylic acid	C7 H7 N O3	154.04948	1.567
27	pos	D-(+)-Proline	C5 H9 N O2	116.07029	1.247
28	pos	PPG n4	C12 H26 O5	251.18465	4.33
29	pos	Pyridoxine	C8 H11 N O3	170.08069	0.825
30	pos	Caffeine	C8 H10 N4 O2	195.0872	3.159
31	pos	4-Pyridoxic acid	C8 H9 N O4	184.05996	1.455
32	pos	Apigenin	C15 H10 O5	271.0594	5.555
33	pos	N-Acetylornithine	C7 H14 N2 O3	175.10717	0.686
34	pos	Cytosine	C4 H5 N3 O	112.05016	0.617
35	pos	2,3,4,9-Tetrahydro-1H-beta-carboline-3-carboxylic acid	C12 H12 N2 O2	217.09672	3.109
36	pos	Ethyl malonate	C5 H8 O4	115.03858	2.548
37	pos	Diisobutyl adipate	C14 H26 O4	259.18967	8.089
38	pos	Fisetin	C15 H10 O6	287.05434	5.413
39	pos	7-Methylguanine	C6 H7 N5 O	166.07184	1.161
40	pos	2-Phenylglycine	C8 H9 N O2	152.07012	2.146

(*Continued*)

Table 1 (Continued).

No.	Ion Mode	Name	Formula	Measured m/z	Retention Times (min)
41	pos	N-Acetylhistamine	C7 H11 N3 O	154.09703	1.028
42	pos	Emodin	C15 H10 O5	271.05942	6.452
43	pos	Uracil	C4 H4 N2 O2	113.03417	1.053
44	pos	L-Pyroglutamic acid	C5 H7 N O3	130.04947	1.169
45	pos	Urocanic acid	C6 H6 N2 O2	139.04977	1.169
46	pos	Methionine	C5 H11 N O2 S	150.0579	1.134
47	pos	Tris(2-butoxyethyl) phosphate	C18 H39 O7 P	399.24974	8.765
48	pos	Leucine	C6 H13 N O2	132.10155	1.476
49	pos	Caffeic acid	C9 H8 O4	181.04911	3.246
50	pos	PPG n5	C15 H32 O6	309.2264	5.005
51	pos	N-Acetyl-L-leucine	C8 H15 N O3	174.11204	3.634
52	pos	L-Kynurenine	C10 H12 N2 O3	209.09155	1.97
53	pos	2'-Deoxyadenosine	C10 H13 N5 O3	252.10837	1.161
54	pos	Citroflex 2	C12 H20 O7	299.10936	5.922
55	pos	Tetraglyme	C10 H22 O5	223.15346	3.29
56	pos	Citroflex 4	C18 H32 O7	383.20305	8.91
57	pos	1-Aminocyclohexanecarboxylic acid	C7 H13 N O2	144.10151	1.623
58	pos	Glycyl-L-leucine	C8 H16 N2 O3	157.09679	1.771
59	pos	Trans-Zeatin	C10 H13 N5 O	220.11727	2.279
60	pos	Delta-Valerolactam	C5 H9 N O	100.07536	2.061
61	pos	N-Acetyl-5-aminosalicylic acid	C9 H9 N O4	196.05997	2.912
62	pos	Alpha-Hydroxyhippuric acid	C9 H9 N O4	196.05985	1.317
63	pos	Bis(methylbenzylidene)sorbitol	C22 H26 O6	387.17922	7.02
64	pos	Nobiletin	C21 H22 O8	403.13771	7.009
65	pos	N-Acetyl-DL-tryptophan	C13 H14 N2 O3	247.10708	4.146
66	neg	Acrylic acid	C3 H4 O2	143.03488	2.4
67	neg	Pyruvic acid	C3 H4 O3	87.00866	0.697
68	neg	L-(+)-Lactic acid	C3 H6 O3	89.02425	1.069
69	neg	Acesulfame	C4 H5 N O4 S	161.98645	1.602
70	neg	Cyclamic acid	C6 H13 N O3 S	178.05408	2.667
71	neg	Quercetin	C15 H10 O7	301.03512	5.064
72	neg	Methylsuccinic acid	C5 H8 O4	131.03491	2.157
73	neg	L-Phenylalanine	C9 H11 N O2	164.07163	2.086

(*Continued*)

Table 1 (Continued).

No.	Ion Mode	Name	Formula	Measured m/z	Retention Times (min)
74	neg	4-Pyridoxic acid	C8 H9 N O4	182.04579	1.466
75	neg	Glutaric acid	C5 H8 O4	131.03492	1.734
76	neg	N-Acetyl-DL-glutamic acid	C7 H11 N O5	188.0563	1.214
77	neg	Caffeic acid	C9 H8 O4	179.03479	3.255
78	neg	3-Hydroxybutyric acid	C4 H8 O3	103.04	1.572
79	neg	Gallic acid	C7 H6 O5	169.01414	1.53
80	neg	Citraconic acid	C5 H6 O4	129.01927	2.023
81	neg	Alpha-Aspartylphenylalanine	C13 H16 N2 O5	279.09836	2.797
82	neg	L-Tyrosine	C9 H11 N O3	180.0665	1.226
83	neg	Xanthohumol	C21 H22 O5	353.13875	7.97
84	neg	2,3-Dihydroxybenzoic acid	C7 H6 O4	153.01924	2.995
85	neg	N-Acetyl-D-alloisoleucine	C8 H15 N O3	172.09785	3.79
86	neg	2-Oxoglutaric acid	C5 H6 O5	145.01412	0.709
87	neg	Adenine	C5 H5 N5	134.04711	1.029
88	neg	Pantothenic acid	C9 H17 N O5	218.10319	2.289
89	neg	Fumaric acid	C4 H4 O4	115.00356	0.694
90	neg	Pimelic acid	C7 H12 O4	159.06622	3.229
91	neg	DL-Lactic Acid	C3 H6 O3	89.0243	0.853
92	neg	3,5-Dihydroxybenzoic acid	C7 H6 O4	153.01926	3.366
93	neg	cis-Aconitic acid	C6 H6 O6	173.00905	0.877
94	neg	N-Acetyl-L-phenylalanine	C11 H13 N O3	206.08213	3.815
95	neg	Suberic acid	C8 H14 O4	173.08183	3.879
96	neg	Levulinic acid	C5 H8 O3	115.04	1.824
97	neg	6-Methoxysalicylic acid	C8 H8 O4	167.03493	1.748
98	neg	3-Methoxysalicylic acid	C8 H8 O4	167.03494	3.928
99	neg	Gentisic acid	C7 H6 O4	153.01917	2.392
100	neg	Vanillic acid	C8 H8 O4	167.0349	2.295
101	neg	Xanthine	C5 H4 N4 O2	151.02603	1.18
102	neg	3-[(1-Carboxyvinyl)oxy]benzoic acid	C10 H8 O5	207.02974	4.265
103	neg	2-Hydroxycaproic acid	C6 H12 O3	131.07126	3.642
104	neg	N-Acetylvaline	C7 H13 N O3	158.08221	3.602
105	neg	cis,cis-Muconic acid	C6 H6 O4	141.01925	2.058
106	neg	Dodecyl sulfate	C12 H26 O4 S	265.14775	7.694

(*Continued*)

https://doi.org/10.2147/CCID.S608837

Table 1 (Continued).

No.	Ion Mode	Name	Formula	Measured m/z	Retention Times (min)
107	neg	2,4-Dihydroxybenzoic acid	C7 H6 O4	153.01922	3.279
108	neg	Isophthalic acid	C8 H6 O4	165.0192	2.376
109	neg	DL-beta-Leucine	C6 H13 N O2	130.08726	1.437
110	neg	3-Hydroxyvaleric acid	C5 H10 O3	117.05565	2.028
111	neg	3-Hydroxy-3-(methoxycarbonyl)pentanedioic acid	C7 H10 O7	205.0352	1.782
112	neg	3-Methylglutaric acid	C6 H10 O4	145.05052	1.505
113	neg	Succinic acid	C4 H6 O4	117.01917	1.262
114	neg	3-Hydroxymandelic acid	C8 H8 O4	167.03488	2.214
115	neg	Kynurenic acid	C10 H7 N O3	188.03519	2.834
116	neg	4-Methylhippuric acid	C10 H11 N O3	192.0665	3.862
117	neg	Saccharin	C7 H5 N O3 S	181.99166	2.054
118	neg	Myristyl sulfate	C14 H30 O4 S	293.17908	8.73
119	neg	4-Oxoproline	C5 H7 N O3	128.03519	1.183
120	neg	Homogentisic acid	C8 H8 O4	167.03491	2.046
121	neg	DL-4-Hydroxyphenyllactic acid	C9 H10 O4	227.05594	3.357
122	neg	Mesaconic acid	C5 H6 O4	111.00865	1.17
123	neg	Isorhamnetin	C16 H12 O7	315.05114	5.808
124	neg	N-Acetyl-4-aminosalicylic acid	C9 H9 N O4	194.04577	3.106
125	neg	Urocanic acid	C6 H6 N2 O2	137.03552	1.18
126	neg	Alpha-Cyano-3-hydroxycinnamic acid	C10 H7 N O3	188.03519	3.755
127	neg	3,4-Dihydroxyphenylpropionic acid	C9 H10 O4	181.05051	2.253
128	neg	2-Methyl-3-hydroxybutyric acid	C5 H10 O3	117.05562	1.811
129	neg	Genipin	C11 H14 O5	207.06615	5.382
130	neg	6-Hydroxypicolinic acid	C6 H5 N O3	138.01955	1.457
131	neg	N-Acetylalanine	C5 H9 N O3	130.05087	1.326
132	neg	Danshensu	C9 H10 O5	179.03488	2.208
133	neg	Esculetin	C9 H6 O4	177.01927	3.26

Abbreviations: pos, positive ion mode; neg, negative ion mode.

Machine Learning Identifies Key Feature Genes

PPI analysis of intersecting targets identified 23 hub targets via Cytoscape and cytoNCA topology analysis (Figure 6A and B). To pinpoint feature genes within the identified targets, LASSO regression, SVM-RFE, and random forest algorithms were employed, resulting in CCNB1 as the key gene (Figure 6C–F).

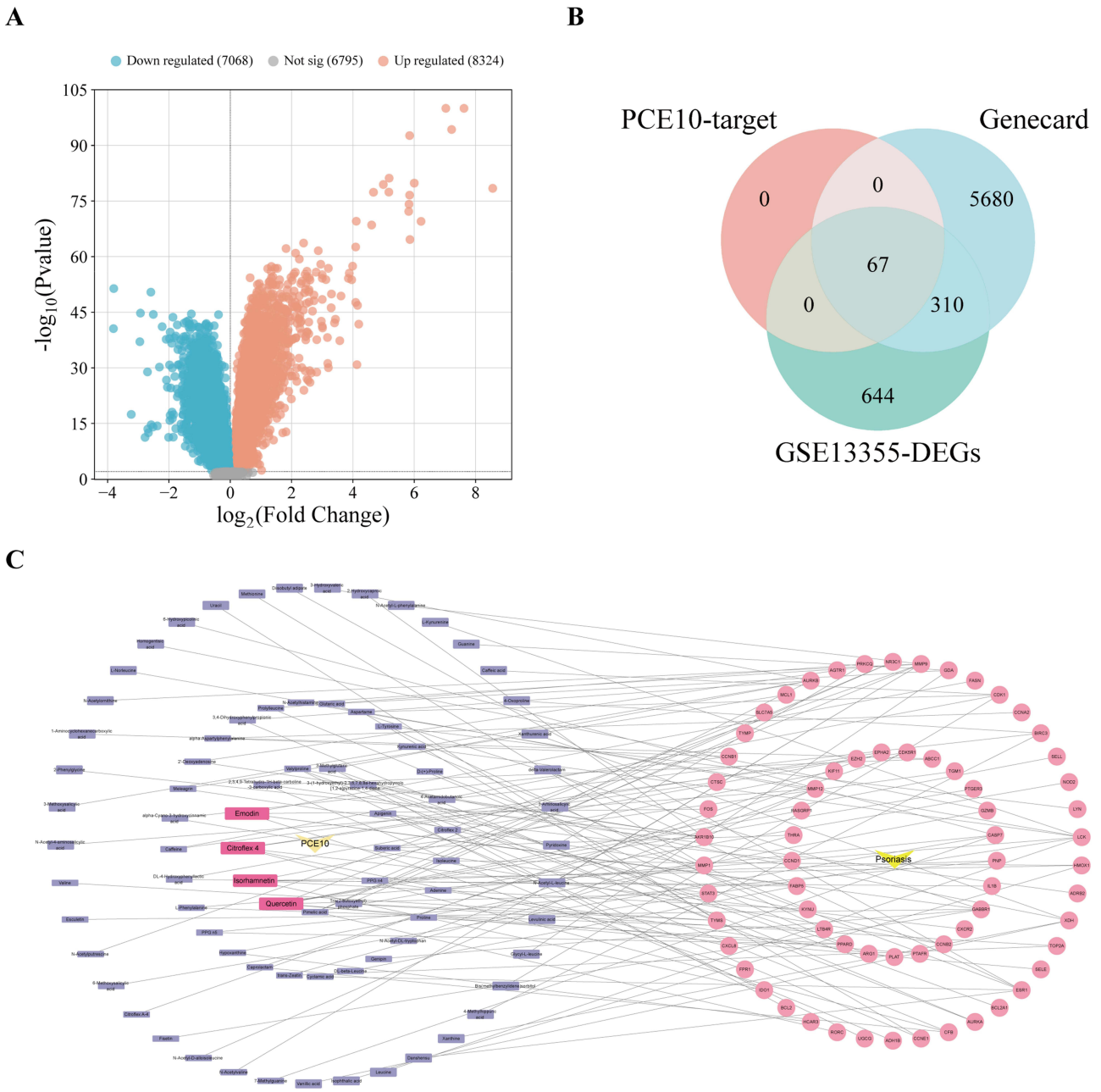

Figure 4 Identification of potential targets of PCE10 in psoriasis. (**A**) Volcano plot of DEGs from GSE13355 dataset. (**B**) Venn diagram of predicted PCE10 targets, DEGs from GSE13355, and disease-related targets from GeneCards. (**C**) Network of PCE10 bioactive components and disease targets.

Interactions Between Active Components and Targets

CCNB1 was mainly enriched in the p53 signaling pathway and cell cycle regulation. Molecular docking analysis suggested potential binding interactions between p53 and core PCE10 components (*quercetin, emodin, isorhamnetin*, and *citroflex 4*) (Figure 7A). IHC showed increased Ki67-positive keratinocytes in IMQ-treated skin, which were reduced by PCE10 in a dose-dependent manner (Figure 7B–C). WB analysis indicated decreased p53 and increased CCNB1 expression in IMQ-treated mice, whereas PCE10 treatment restored p53 levels and suppressed CCNB1 expression across all doses (Figure 7D–E).

https://doi.org/10.2147/CCID.S608837

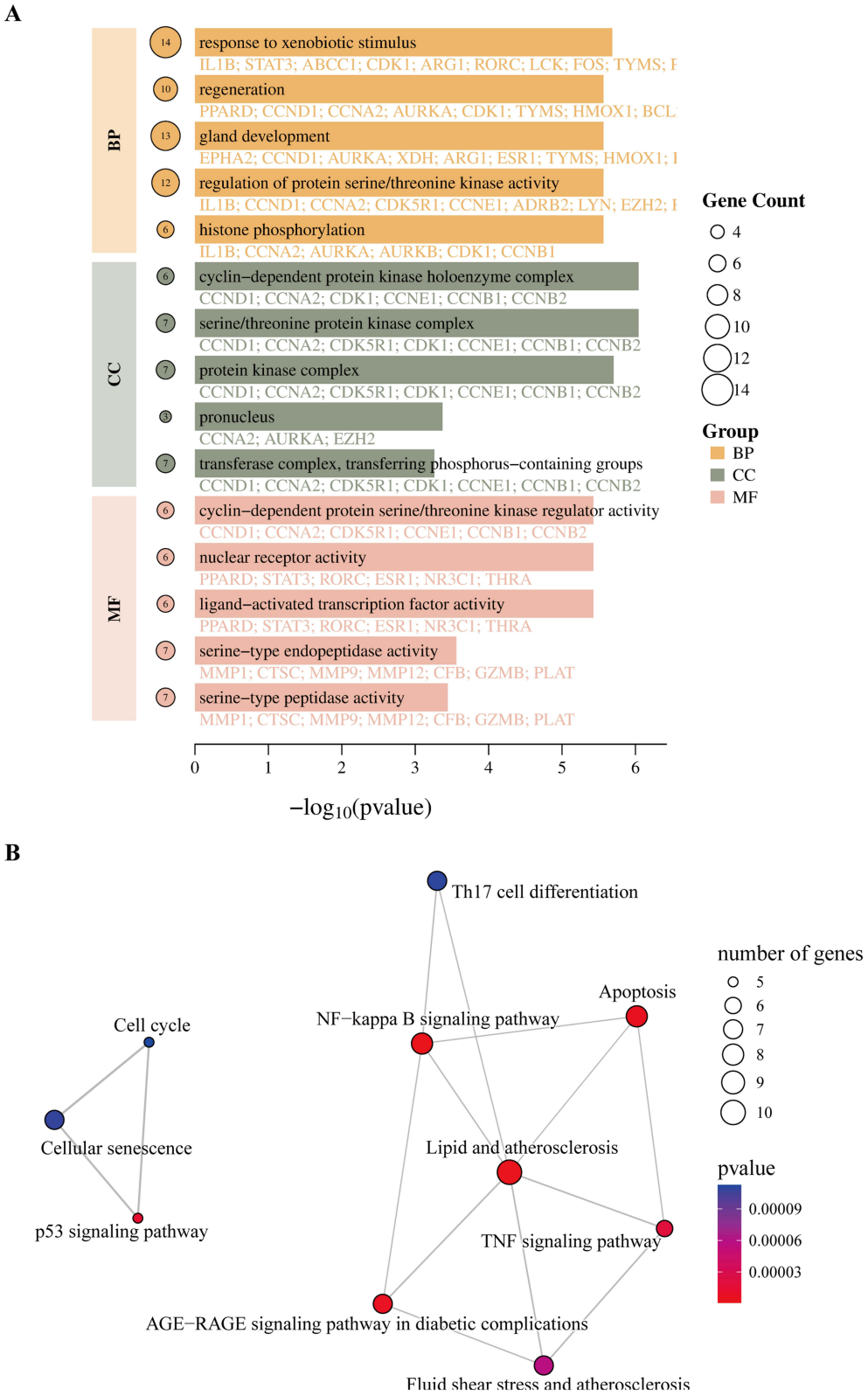

Figure 5 GO and KEGG enrichment analyses of drug–disease targets. (**A**) GO annotation of drug–disease targets. (**B**) KEGG pathway annotation of drug–disease targets.

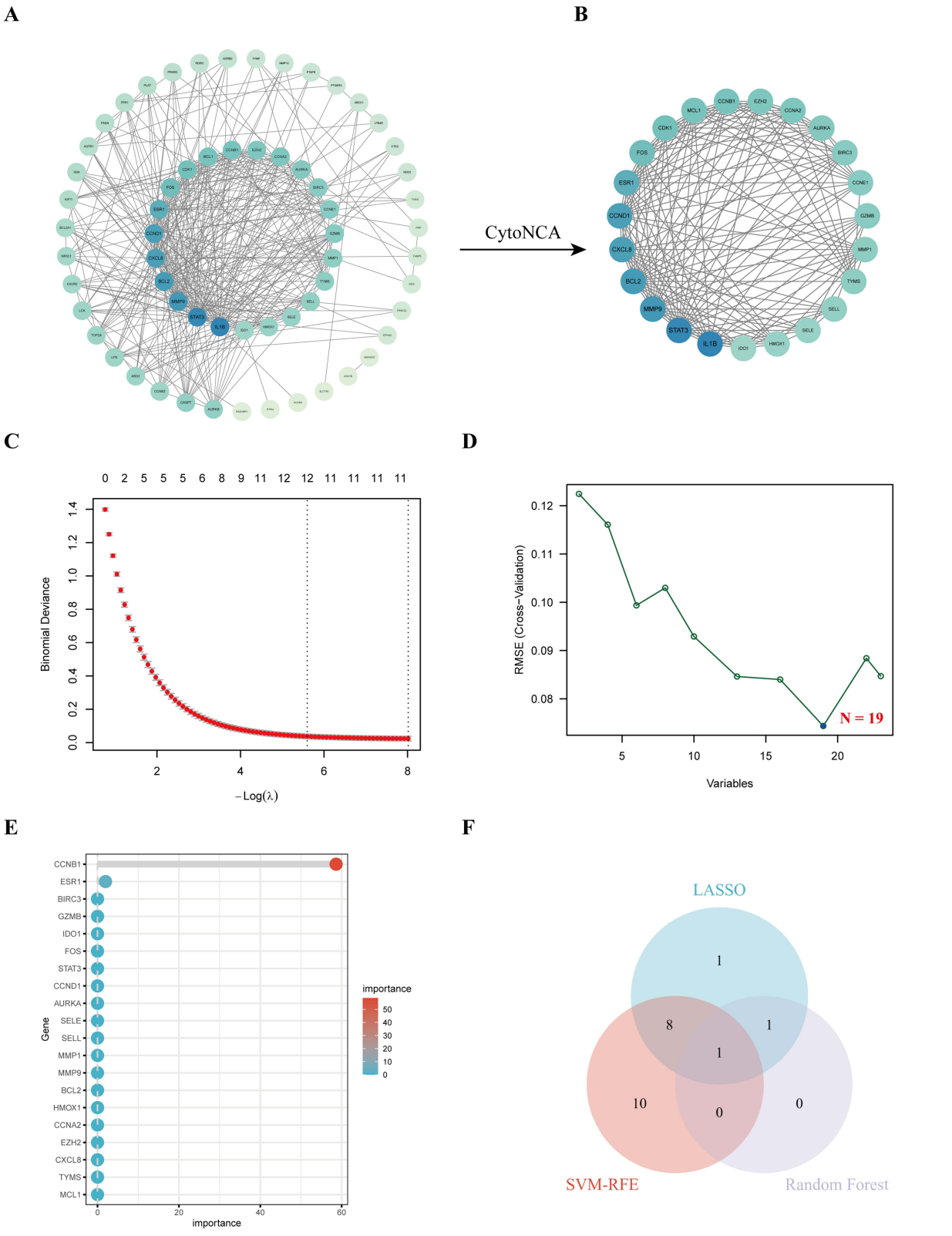

Figure 6 Machine learning-based screening of PPI core targets. (**A**) PPI network of core targets. (**B**) Key targets identified using CytoNCA plugin. (**C**) LASSO regression results of feature targets. (**D**) SVM-RFE results of feature targets. (**E**) Random forest results of feature targets. (**F**) Venn diagram showing intersecting results of LASSO, SVM-RFE, and random forest analyses.

https://doi.org/10.2147/CCID.S608837

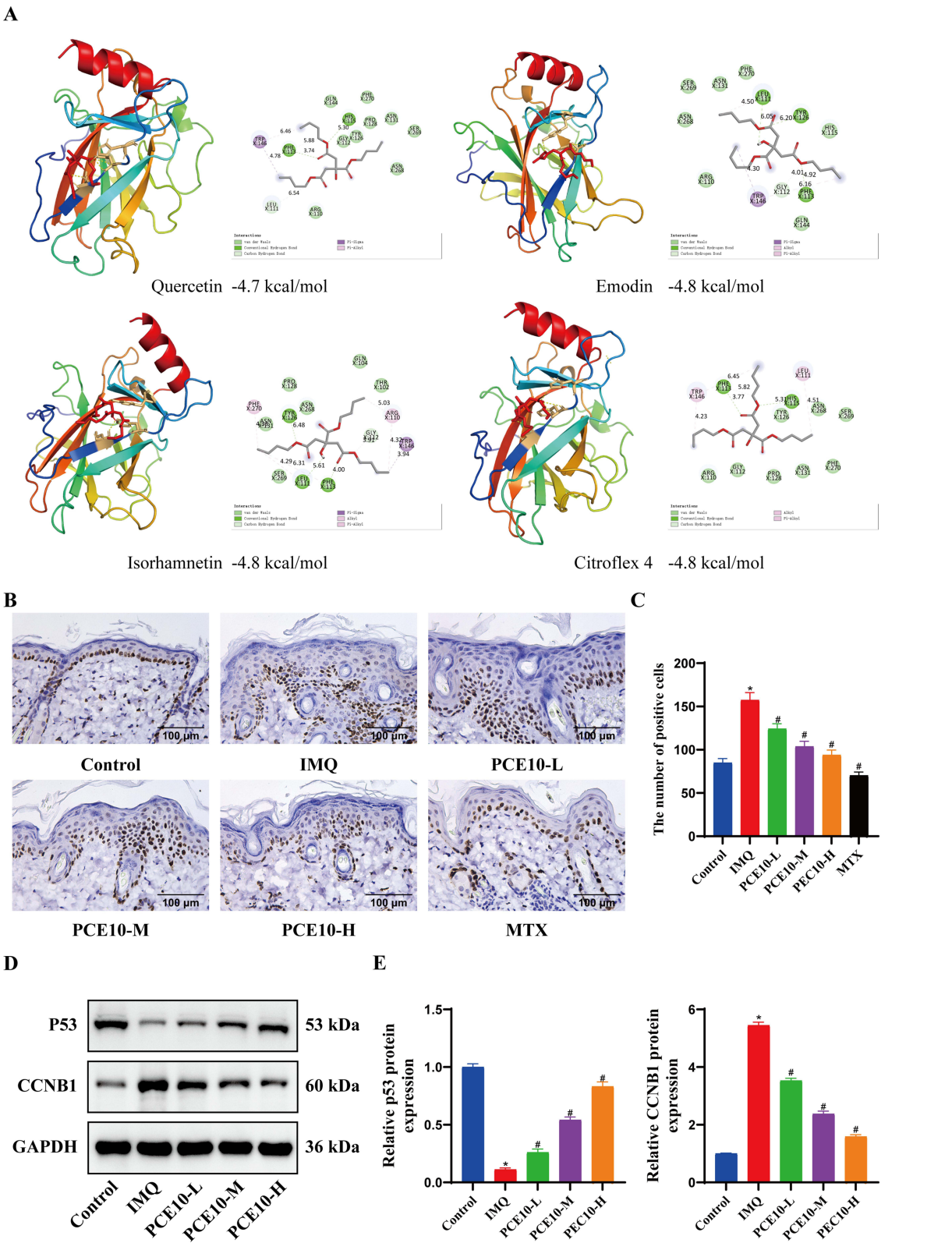

Figure 7 Molecular docking of key targets and core compounds. (**A**) Molecular docking of p53 with core compounds. (**B**) IHC detection of Ki67 expression in skin. (**C**) Quantification of Ki67-positive cells. (**D**) WB analysis of p53 and CCNB1 expression in tissue. (**E**) Quantification of protein expression. Data analyzed by one-way ANOVA with Tukey's post hoc test. n = 6 mice per group; *p < 0.05 vs Control; #p < 0.05 vs IMQ.

https://doi.org/10.2147/CCID.S608837

Discussion

Psoriasis is increasingly recognized as a multifactorial inflammatory disorder involving dysregulated immune responses and abnormal keratinocyte proliferation, which has prompted growing interest in multi-target therapeutic strategies.[4] In recent years, natural bioactive compounds have attracted attention for their ability to modulate inflammatory pathways and cellular proliferation simultaneously.[14] Such properties suggest that plant-derived compounds may represent promising complementary approaches for the management of chronic inflammatory skin diseases such as psoriasis. In our study, we demonstrate that PCE10, the ethanol extract of *Prunus cerasifera* fruit powder, may exert anti-inflammatory effects on psoriasis.

Our results showed that PCE10 significantly alleviated IMQ-induced psoriasis-like skin inflammation in mice. Consistently, previous studies have also demonstrated that *Prunus cerasifera* extracts possess significant anti-inflammatory activity by suppressing pro-inflammatory cytokine production.[15] In addition, extracts of Prunus species are rich in phenolic and flavonoid compounds with strong antioxidant and skin-protective effects,[16] suggesting their potential utility in managing inflammatory skin disorders. Importantly, the therapeutic effects of PCE10 exhibited dose-dependency. Mice receiving medium (150 mg/kg/day) and high (300 mg/kg/day) doses showed more pronounced improvement in PASI scores, epidermal thickness, and inflammatory markers compared to the low-dose group (75 mg/kg/day). These findings highlight the necessity of optimizing dosage for potential clinical translation, balancing efficacy with safety, and may inform future studies on pharmacokinetics and dose-response relationships of *Prunus cerasifera* extracts.

Furthermore, this study revealed that *quercetin, emodin, isorhamnetin*, and *citroflex 4* were core bioactive components of PCE10. These findings align with previous studies indicating the therapeutic potential of natural flavonoids and anthraquinones in inflammatory skin disorders.[17] *Quercetin, emodin*, and *isorhamnetin* have been reported to possess anti-inflammatory and antioxidant properties, attenuating keratinocyte hyperproliferation and cytokine release in various in vitro and in vivo models. Specifically, *Quercetin* suppresses TNF-α and IL-17A-mediated signaling in keratinocytes.[18] *Emodin* modulates NF-κB and MAPK pathways,[19] while *isorhamnetin* exerts regulatory effects on cell cycle proteins in proliferative skin conditions.[20] *Citroflex 4*, though less studied, was identified as a core bioactive component in our network analysis and may synergistically enhance the anti-proliferative and anti-inflammatory effects of the other compounds, representing a novel therapeutic contribution.

Mechanistically, our integrated analyses suggested that PCE10 may exert its therapeutic effects through the p53/CCNB1 axis. Molecular docking analysis indicated potential binding interactions between key PCE10 components and p53, providing preliminary support for this regulatory pathway. The tumor suppressor p53 is crucial for regulating keratinocyte proliferation and controlling the cell cycle, and its expression has been reported to be significantly increased in psoriatic lesions compared with normal skin,[21] suggesting its involvement in epidermal hyperproliferation and inflammatory responses. Suppression of p53 signaling in keratinocytes can exacerbate psoriasis by promoting uncontrolled cellular proliferation,[22] highlighting the importance of the p53-mediated regulatory network in maintaining epidermal homeostasis. Additionally, CCNB1 has been identified as a potential biomarker and pathogenic factor in psoriasis, where it may influence keratinocyte proliferation.[23] These findings indicate that the p53/CCNB1 signaling axis plays a critical role in regulating keratinocyte proliferation and inflammatory responses in psoriasis. The observed reduction of IL-17A, TNF-α, and IL-23 levels in our study further supports the mechanism of action.

Compared with conventional systemic therapies such as MTX, PCE10 demonstrated comparable anti-inflammatory and anti-proliferative effects in the IMQ-induced psoriasis model, although through potentially different molecular mechanisms. MTX has long been considered a first-line systemic therapy for moderate-to-severe psoriasis and primarily acts by suppressing immune activation and inducing apoptosis in hyperproliferative keratinocytes.[24] Previous studies have shown that MTX promotes keratinocyte apoptosis through activation of the intrinsic apoptotic pathway, accompanied by increased cytochrome c release and caspase-9 activation while suppressing pro-survival signaling pathways such as NF-κB and Akt in psoriatic lesions.[25] These mechanisms ultimately reduce epidermal hyperplasia and inflammatory responses. Nevertheless, prolonged administration of MTX is frequently linked with side effects, including hepatotoxicity, gastrointestinal disturbances, and immunosuppressive complications, which limits its prolonged clinical use.[26] In contrast, natural bioactive compounds derived from plant sources may exert therapeutic effects through multi-target regulatory mechanisms with potentially improved safety profiles.[27] In the present study, *quercetin, emodin*, and *isorhamnetin*, PCE10 core components, may suppress key inflammatory mediators. Unlike MTX, which primarily acts through immunosuppressive and cytotoxic

effects on rapidly dividing cells, these natural components may regulate multiple signaling pathways simultaneously, thereby restoring epidermal homeostasis while attenuating inflammatory signaling.

Despite these promising results, there are several limitations. First, this study relied exclusively on an IMQ-induced mouse model, which does not fully replicate the chronic, heterogeneous pathophysiology of human psoriasis. Additionally, we lacked validation using human psoriatic skin tissues or clinical samples. Future studies should employ complementary models (eg., human keratinocyte cultures, skin equivalents, or genetic mouse models) and incorporate human tissue validation to improve translational relevance. Second, deeper mechanistic experiments are needed. While network pharmacology and molecular docking predicted interactions between PCE10 components and p53/CCNB1, these in silico findings require experimental validation. Predicted binding energies ranged from −4.0 to −5.0 kcal/mol, indicating moderate binding potential, and should be interpreted with caution. Future studies should employ biochemical assays (eg., SPR, CETSA, or DARTS) to confirm direct compound-target interactions, along with functional rescue experiments (eg., p53 knockdown or CCNB1 overexpression) to establish causality. Third, while machine learning identified CCNB1 as a key target, other potential pathways and off-target effects of PCE10 remain unexplored. Future multi-omics approaches (transcriptomics, proteomics) combined with functional validation will help comprehensively elucidate the molecular mechanisms of PCE10. Furthermore, the PCE10 extract contains 230 identified components, and the synergistic or antagonistic interactions among them require further investigation. Long-term safety and efficacy in chronic psoriasis models also remain to be assessed. Finally, a systematic comparative evaluation of different elution fractions was not performed in this study. While we identified PCE10 as an active fraction, it remains unclear whether other fractions possess distinct or superior therapeutic properties. Future research should compare the efficacy, safety, and mechanism of action across multiple elution fractions to optimize the extraction strategy.

Overall, our study provides novel evidence that PCE10, through the combined action of its core components, can regulate key proliferative and inflammatory pathways in psoriasis. These results broaden the therapeutic applicability of *Prunus cerasifera* extracts and reinforce the potential of natural multi-target strategies for managing chronic inflammatory skin disorders. Further investigations are needed to clarify the pharmacokinetic profiles, long-term therapeutic outcomes, and possible synergistic interactions of these bioactive constituents in clinical contexts.

Data Sharing Statement

All data are available from the corresponding author upon reasonable request.

Ethics Statement

All animal procedures were approved by the Ethics Committee of People's Hospital of Xinjiang Uygur Autonomous Region (approval no. KY2024102201).

Funding

This study was supported by Xinjiang Uygur Autonomous Region Central Government Guides Local Science and Technology Development Fund Project (Project No. ZYYD2025JD13); Xinjiang Uygur Autonomous Region Tianshan Talent Program - Youth Top notch Talent Project (Project No. 2024TSYCCX0078); First-class scientific and technological leaders in the Xinjiang Strategic Talent Development Plan (Project No. XJRC-2025-KJ-PY-KJLJ-113).

Disclosure

The authors declare no competing interests.

References

1. Armstrong AW, Blauvelt A, Callis Duffin K, et al. Psoriasis. *Nat Rev Dis Primers*. 2025;11(1):45. doi:10.1038/s41572-025-00630-5
2. Metyas S, Tomassian C, Messiah R, Gettas T, Chen C, Quismorio A. Combination therapy of apremilast and biologic agent as a safe option of psoriatic arthritis and psoriasis. *Curr Rheumatol Rev*. 2019;15(3):234–237. doi:10.2174/1573397115666181130094455
3. Rendon A, Schakel K. Psoriasis pathogenesis and treatment. *Int J Mol Sci*. 2019;20(6). doi:10.3390/ijms20061475
4. Sugumaran D, Yong ACH, Stanslas J. Advances in psoriasis research: from pathogenesis to therapeutics. *Life Sci*. 2024;355:122991. doi:10.1016/j.lfs.2024.122991

5. Ghoreschi K, Balato A, Enerback C, Sabat R. Therapeutics targeting the IL-23 and IL-17 pathway in psoriasis. *Lancet*. 2021;397(10275):754–766. doi:10.1016/S0140-6736(21)00184-7
6. Zou Y, Meng Z. Literature overview of the IL-17 inhibition from psoriasis to COVID-19. *J Inflamm Res*. 2021;14:5611–5618. doi:10.2147/JIR.S329252
7. Bakshi H, Nagpal M, Singh M, Dhingra GA, Aggarwal G. Treatment of psoriasis: a comprehensive review of entire therapies. *Curr Drug Saf*. 2020;15(2):82–104. doi:10.2174/1574886315666200128095958
8. Han L, Ho CT, Lu M. Regulatory role of bioactive compounds from natural spices on mitochondrial function. *J Agric Food Chem*. 2025;73(10):5711–5723. doi:10.1021/acs.jafc.4c12341
9. Silvan JM, Michalska-Ciechanowska A, Martinez-Rodriguez AJ. Modulation of antibacterial, antioxidant, and anti-inflammatory properties by drying of *Prunus domestica* L. plum juice extracts. *Microorganisms*. 2020;8(1). doi:10.3390/microorganisms8010119
10. Magiera A, Czerwinska ME, Owczarek A, Marchelak A, Granica S, Olszewska MA. Polyphenol-Enriched extracts of prunus spinosa fruits: anti-inflammatory and antioxidant effects in human immune cells ex vivo in relation to phytochemical profile. *Molecules*. 2022;27(5). doi:10.3390/molecules27051691
11. Qiao Y, Li C, Chen C, et al. Multi-Target mechanism of compound qingdai capsule for treatment of psoriasis: multi-omics analysis and experimental verification. *Drug Des Devel Ther*. 2025;19:5209–5230. doi:10.2147/DDDT.S523836
12. Li AH, Chen YQ, Chen YQ, Song Y, Li D. CCNB1 and CCNB2 involvement in the pathogenesis of psoriasis: a bioinformatics study. *J Int Med Res*. 2022;50(8):3000605221117138. doi:10.1177/03000605221117138
13. Chen L, Qi X, Wang J, et al. Identification of novel candidate genes and predicted miRNAs in atopic dermatitis patients by bioinformatic methods. *Sci Rep*. 2022;12(1):22067. doi:10.1038/s41598-022-26689-8
14. Roy T, Boateng ST, Uddin MB, et al. The PI3K-Akt-mTOR and associated signaling pathways as molecular drivers of immune-mediated inflammatory skin diseases: update on therapeutic strategy using natural and synthetic compounds. *Cells*. 2023;12(12). doi:10.3390/cells12121671
15. Zagorska-Dziok M, Ziemlewska A, Wojciak M, Sowa I, Wasik-Szczepanek E, Niziol-Lukaszewska Z. Comparison of cytotoxicity and antioxidant, antibacterial, and anti-inflammatory activity of aqueous and ethanolic extracts from *Malus domestica*, *Prunus armeniaca*, and *Prunus cerasus* leaves. *Molecules*. 2025;30(10). doi:10.3390/molecules30102085
16. Mungmai L, Wongwad E, Tanamatayarat P, et al. Stability, bioactivity, and skin penetration of prunus leaf extracts in cream formulations: a clinical study on skin irritation. *Cosmetics*. 2025;12(4):146.
17. Lee SK, Keng JW, Yon JA, et al. Phytochemical analysis and biological activities of flavonoids and anthraquinones from *Cassia alata* (Linnaeus) roxburgh and their implications for atopic dermatitis management. *Plants*. 2025;14(3). doi:10.3390/plants14030362
18. Chen BL, Zhang WM, Dong XW, Liu JY, Bai YP. Quercetin induces keratinocytes apoptosis via triple inhibition of notch, PI3K/AKT signaling and Glut1 in the treatment of psoriasis. *Biochim Biophys Acta Mol Basis Dis*. 2025;1871(6):167879. doi:10.1016/j.bbadis.2025.167879
19. Nguyen LTH, Ahn SH, Shin HM, Yang IJ. Anti-Psoriatic effect of rheum palmatum l. and its underlying molecular mechanisms. *Int J Mol Sci*. 2022;23(24). doi:10.3390/ijms232416000
20. Wu J, Song Y, Wang J, et al. Isorhamnetin inhibits hypertrophic scar formation through TGF-beta1/Smad and TGF-beta1/CREB3L1 signaling pathways. *Heliyon*. 2024;10(13):e33802. doi:10.1016/j.heliyon.2024.e33802
21. Mercurio L, Bailey J, Glick AB, et al. RAS-activated PI3K/AKT signaling sustains cellular senescence via P53/P21 axis in experimental models of psoriasis. *J Dermatol Sci*. 2024;115(1):21–32. doi:10.1016/j.jdermsci.2024.03.002
22. Wang N, Xu X, Guan F, et al. FGF12 positively regulates keratinocyte proliferation by stabilizing MDM2 and inhibiting p53 activity in psoriasis. *Adv Sci*. 2024;11(39):e2400107. doi:10.1002/advs.202400107
23. Ding J, Sun A, Hu H, et al. Potential targets and mechanisms of saikosaponin D in psoriasis: a bioinformatic and experimental study on oxidative stress. *J Inflamm Res*. 2025;18:16487–16507. doi:10.2147/JIR.S563272
24. Lang Houser ME, Stewart JR, Brewer JD. Psoriasis patients treated with methotrexate have an increased risk of nonmelanoma skin cancer: a systematic review and meta-analysis. *Cureus*. 2023;15(4):e37174. doi:10.7759/cureus.37174
25. van Huizen AM, Sikkel R, Caron AGM, Menting SP, Spuls PI. Methotrexate dosing regimen for plaque-type psoriasis: an update of a systematic review. *J DermatolTreat*. 2022;33(8):3104–3118. doi:10.1080/09546634.2022.2117539
26. Chan BS, Bosco AA, Buckley NA. Navigating methotrexate toxicity: examining the therapeutic roles of folinic acid and glucarpidase. *Br J Clin Pharmacol*. 2025;91(3):628–635. doi:10.1111/bcp.16096
27. Zhao W, Yang A, Wang J, et al. Potential application of natural bioactive compounds as skin-whitening agents: a review. *J Cosmet Dermatol*. 2022;21(12):6669–6687. doi:10.1111/jocd.15437